PREDICTION AND MEASUREMENT OF FLOW-INDUCED WALL-PRESSURE FLUCTUATIONS AT LOW MACH NUMBERS

Jared Van Blitterswyk* and Joana Rocha†
Department of Mechanical and Aerospace Engineering, Carleton University, Ottawa, Ontario

Abstract

Flow-induced wall-pressure fluctuations, on a single panel, in a wind tunnel environment are measured and analyzed for Mach numbers between 0.06 and 0.12. The effects of two, flush-mounted microphone cap configurations on measured wall pressure spectra are investigated. A selection of semi-empirical single-point frequency spectrum models, are reviewed and compared to experimental wall-pressure spectra. The measured wall-pressure spectra are compared in dimensional and non-dimensional forms to investigate dependencies on Mach number and turbulent boundary layer scaling variables. The spectra captured with the pinhole microphone configuration are in better agreement with expected behaviour presented in the literature, compared to the grid cap configuration, but show a greater Mach number dependency when scaled with mixed inner and outer boundary layer variables. The models by Laganelli and Efimtsov are most suitable for predicting wall-pressure amplitudes over the low- and mid-frequency regimes whereas, the more recent models by Smol'yakov and Goody are most appropriate for predicting the decay rate in the overlap regime. The absence of a sizeable overlap region, caused by an under-developed logarithmic region in the boundary layer, is responsible for the disparities between measured and predicted spectra, and the Mach number dependence shown by the normalized spectra.

Keywords: turbulent boundary layer, wall-pressure fluctuations, wind tunnel, semi-empirical models, rigid panel

Résumé

Les fluctuations de la pression au mur induites par l'écoulement sur un panneau seul, dans un environnement de soufflerie, ont été mesurées et analysées contre les nombres de Mach entre 0,06 et 0,12. Les effets des spectres de pression mesurés au mur pour deux configurations d'encastrement des microphones ont été étudié. Une sélection de modèles de spectres semi-empiriques mono point en fréquence a été examinées et comparés aux spectres expérimentaux de pression au mur. Les spectres de pression au mur mesurés ont été comparés, dans leur formes dimensionnelles et non dimensionnelles, pour afin de déterminer l'influence du nombre de Mach et les variables de mise à l'échelle de la couche limite turbulente. Les spectres capturés avec la configuration du microphone sténopé son en meilleur accord avec le comportement attend, présenté dans la littérature, par rapport à la configuration avec cap de protection, mais montrent une plus grande dépendance au nombre de Mach lorsque mise à l'échelle des variables mixtes de la couche limite intérieure et extérieure. Les modèles de Laganelli et Efimtsov sont plus acceptable pour prédire les amplitudes de la pression au mur pour les régimes a basses et moyennes fréquences, tandis que les modèles plus récents par Smol'yakov et Goody conviennent mieux pour prédire le taux de désintégration du régime du chevauchement. L'absence d'une région de chevauchement considérables, causé par une région sous-développée logarithmique dans la couche limite, est responsable des disparités entre les spectres mesurés et prédits et l'influence du nombre de Mach, illustré par les spectres normalisés.

Mots clefs : couche limite turbulente, les fluctuations de pression au mur, soufflerie, modèles semi-empiriques, panneau rigide

* jaredvanblitterswyk@cmail.carleton.ca
† Joana.Rocha@carleton.ca

Nomenclature

C_f = skin friction coefficient
f = frequency
h_{aw} = enthalpy at the wall – adiabatic conditions
h_w = enthalpy at the wall
L = coherence length of the boundary layer
M = Mach number
p = instantaneous wall-pressure amplitude
$\overline{P^2}$ = mean-square pressure
q_∞ = dynamic pressure
Re_x = Reynolds number based on distance
Re_τ = Reynolds number based on wall shear stress
Re_θ = Reynolds number based on momentum thickness
U_c = convection velocity
U_τ = friction velocity
U_∞ = freestream velocity
x = distance from start of test section
γ = specific heat ratio of air
Γ = cross-spectra
δ = boundary layer thickness
δ^* = displacement thickness
ξ = spatial separation between points of interest on panel
θ = momentum thickness
ν = kinematic viscosity
ρ = freestream density
τ_w = wall shear stress
Φ = auto-spectra
ω = angular frequency

1 Introduction

The characterization and prediction of Turbulent Boundary Layer (TBL)-induced sound for aircraft applications has been investigated for several years. A comprehensive review of pertinent investigations are summarized by Bull [1]. The advent of more advanced technologies have increased cruise flight speeds of commercial and recreational aircraft. It has been shown that a primary source of cabin noise during cruise conditions is induced by the TBL wall-pressure fluctuations [2]. These pressure fluctuations act as a forcing function to the exterior skin panels which vibrate in response, radiating an acoustic signature inwards to the cabin. Significant amplification of the overall radiated sound pressure levels can occur under circumstances where excitations from turbulent eddy structures match the longitudinal/lateral trace speed of resonant vibration modes of airframe skin panels, known as aerodynamic coincidence [3]. Coincidence can theoretically occur at any speed; however, it has been shown that coincidence does not become a concern until mid-subsonic/transonic Mach numbers [3]. Even in cases where aerodynamic coincidence does not occur, mid- and high-frequency TBL excitations represent a significant portion of the overall cabin sound pressure levels [4]. These excitations span the predominant frequency range to which humans are most affected; excessive noise can cause passenger and crew discomfort, health related issues, malfunction of electronic equipment and verbal communication interference [2].

An active field of research is the characterization of cabin noise, as a function of the boundary layer parameters. Early experimental investigations focused on characterizing the wall-pressure spectra for a single panel excited by a TBL [5-9]. These studies provided insight into the expected shape of the spectrum with varying flow conditions. The wall-pressure spectrum, in the frequency domain, is commonly characterized by four frequency ranges, in which the spectrum has an approximate power law behaviour; the ranges of low-frequency ($f <$ 65 Hz), mid-frequency (65 Hz < f < 650 Hz), overlap (1.3 kHz < f 55 kHz), and high-frequency ($f >$ 55 kHz). It is common practice in boundary layer analyses to normalize by parameters of the boundary layer and the applicability to spectral analyses of wall-pressure fluctuations has been thoroughly investigated [7,8,10-12]. Scaling is based on the concept that the spectrum exhibits self-similarity and will retain its key features over a vast range of flow conditions. Unfortunately, due to the dynamic behaviour of a TBL, a single set of boundary layer parameters which collapses the spectrum over the entire range of pertinent frequencies, has yet to be found. However, various sets of parameters have been shown to collapse specific regions of the spectrum [1,8,10].

Many authors have attempted further characterization by generating semi-empirical models, which predict the behaviour of wall-pressure fluctuations. Over the years, three types of models have emerged: root mean-square pressure models, wavenumber-frequency spectrum models, and single point wall-pressure frequency spectrum models.

Root mean-square pressure models use the amplitude of pressure fluctuations to describe the energy beneath a TBL. These models have the advantage of condensing the complete frequency response down to a single representative pressure value, which describes the intensity of the process. However, being the integration of a single-point frequency spectrum, these models accumulate greater error than individual sound pressure levels described in the form of a frequency spectrum and, therefore, are less preferred [1]. Wavenumber models reveal details about flow convection and concentrated spectral energy, which influence the structural response of a panel. Wavenumber models can be particularly useful in the design stage for formulating design criteria for the mitigation of aerodynamic coincidence effects. Single-point frequency spectrum models are similar to wavenumber models in that they describe the distribution of mean-square pressure levels, but in the frequency domain. Frequency spectrum models are useful for identifying the dominant frequencies in a TBL, evaluating the frequency response of a panel to TBL excitations and describing the spectral energy in a context easily relatable to the human perception of sound.

More advanced analytical frameworks for continuum models [13,14], and the numerical approaches of Statistical Energy Analysis (SEA) or Dynamic Energy Analysis (DEA), bridge the prediction of airborne and structure-borne sound levels to predict the transmission of sound and vibration through complex acoustic structures, such as an

aircraft fuselage. Finite element methods can also be applied, although solutions can be computationally expensive [2]. Regardless of the approach employed, single-point frequency spectrum models are an integral component as they provide the frequency distribution of the TBL excitation at each point on the exterior surface of the structure in question. Therefore, there is a need to comparatively evaluate the appropriateness of existing models to predict the spectra of wall-pressure fluctuations beneath a TBL.

Two comprehensive studies by [15,16] concluded that the model by Goody is in the best agreement with experimentally measured wall-pressure spectra at low Mach numbers, although neither reported a single model which predicted the spectra over the entire frequency range. The data sets collected in [16] were contaminated by noise at high frequencies, thus limiting the comparisons to frequencies below 2.5 kHz. The comparative study in [15] featured multiple data sets from the literature, covering a more extensive frequency range, but comparisons were still limited to frequencies below 7 kHz.

The present study investigates a more complete frequency range, in which comparisons are made to existing wall-pressure spectrum semi-empirical models using predicted flow properties. The single-point frequency spectrum models in consideration include models by: Efimtsov [17], Rackl and Weston [18], Lowson [19], Robertson [20], Laganelli [21], Goody [11] and Smol'yakov [12]. Additionally, the effects of two microphone cap configurations on the measured frequency spectra, and the dependence of the normalized spectrum shape on Mach number and predicted boundary layer properties, are investigated.

2 Semi-Empirical Models

Given the stochastic nature of a TBL, the wall-pressure fluctuations developed over a flat panel are usually described statistically. Single-point frequency spectrum, or auto-spectra, models describe wall-pressure fluctuations using the Power Spectral Density (PSD). Many authors have developed models to predict the PSD of TBL-induced wall-pressure fluctuations, assuming fully developed flow with a zero-mean pressure gradient, which allows the flow to be considered stationary and homogenous in the plane of the wall. An assumption with current semi-empirical models is that the aerodynamic excitation can be treated in isolation from the structure. The auto-spectra, $\Phi(f)$, is commonly used in cross-spectral analyses, where the coherent power ([…] in Eq. (1)) of the wall-pressure fluctuations can be described using Corcos formulation [22,23] as:

$$\Gamma(\xi_x, \xi_y, f) = \Phi(f)\left[e^{-\left|\frac{\xi_x}{L_x}\right|} e^{-\left|\frac{\xi_y}{L_y}\right|} e^{-\frac{\mathrm{i}2\pi f \xi_x}{U_c}}\right] \quad (1)$$

In the current study, the applicability of various existing semi-empirical models to predict the auto-spectra at low Mach number flows, was investigated. The experimental wall-pressure spectra were compared to six semi-empirical models developed by: Efimtsov [17], Rackl and Weston [18], Lowson [19], Robertson [20], Laganelli [21], Goody [11] and Smol'yakov [12]. The survey of models discussed in the following sections is not meant to serve as an exhaustive list, but more a review of the more popular models. The reader is encouraged to review the cited works for a more detailed description of the models.

2.1 Efimtsov's Model [17]

Efimtsov developed two models using extensive flight testing and wind tunnel experiments, covering a range of subsonic and supersonic Mach numbers. The second, more recent, model will be considered. Using Reynolds number and Strouhal number, Sh, as independent variables, Efimtsov proposed the following semi-empirical model (Eq. (2)),

$$\Phi(f) = 2\pi\alpha {U_\tau}^3 \rho^2 \delta \frac{\beta}{(1 + 8\alpha^3 Sh^2)^{\frac{1}{3}} + \alpha\beta Re_\tau \left(\frac{Sh}{Re_\tau}\right)^{\frac{10}{3}}} \quad (2)$$

where;

$$\alpha = 0.01\ , \beta = \left[1 + \left(\frac{Re_{\tau o}}{Re_\tau}\right)^3\right]^{\frac{1}{3}},\ \ Sh = 2\pi f \delta / U_\tau$$

$$U_\tau = U_\infty \sqrt{\frac{C_f}{2}}\ , Re_\tau = \frac{\delta U_\tau}{\nu_w}, Re_{\tau o} = \frac{\delta U_\tau}{\nu}$$

The coefficient of friction, C_f, and boundary layer thickness, δ, were predicted using the following relations from [24] and [25], respectively.

$$C_f = 0.37\left(\log_{10} R_{e_x}\right)^{-2.584} \quad (2a)$$

$$\delta = 0.37 x {R_{e_x}}^{-\frac{1}{5}}[1 + 0.144M^2]^{0.35} \quad (2b)$$

2.2 Rackl and Weston's Model [18]

Rackl and Weston developed correction functions for Efimtsov's second model (Eq. (2)), based on flight test measurements on a Tu-144LL supersonic aircraft. The resulting form of the single point frequency spectrum has the form of Eq. (3).

$$\Phi'(f) = \Phi(f) + \chi_1(f) + \chi_2(f) \quad (3)$$

The correction functions, $\chi_1(f)$ and $\chi_2(f)$ in Eq. (3), adjust the high frequency roll-off response (Eq. (4a)), and capture the broad band peak around a Strouhal number of 0.6 (Eq. (4b)).

$$\chi_1(f) = \frac{1}{4}\left[\tanh\left(\log_{10}\left(\frac{f}{1000}\right)\right) + 1\right][M - 1.65]\log_{10}(f) \quad (4a)$$

$$\chi_2(f) = 2.5 e^{\left(-\left(\ln\left(\frac{2\pi\delta^*}{U_o}(f)\right) - \ln(0.6)\right)^2\right)} \quad (4b)$$

The displacement thickness, δ^*, was estimated using Eq. (4) [25].

$$\delta^* = \delta(x)\left\{1 - \frac{1.88(\log_{10}(R_{e_x}) - 3.06)}{1.88(\log_{10}(R_{e_x}) - 4.752)(1 + 0.065M^2)}\right\} \quad (4)$$

These correction factors were calculated for each Mach number using predicted TBL properties for the current experimental setup. Fig. 1 shows the correction factors over the frequency range of 10 Hz < f < 10 kHz for conditions at M = 0.12.

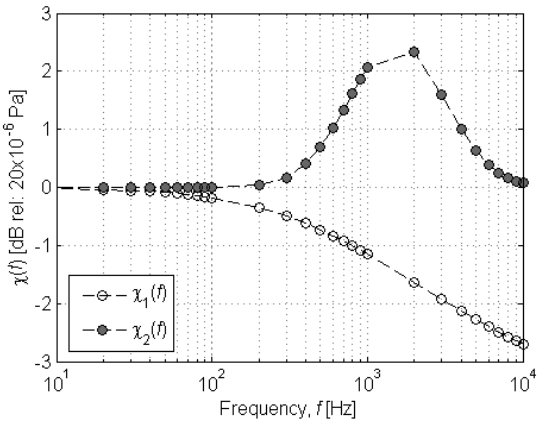

Figure 1: Auto-spectra correction factors postulated by Rackl and Weston [18] for M = 0.12 test conditions

2.3 Lowson's Model [19]

Lowson developed a semi-empirical model, which closely matched the empirical curves developed by Bies [26], and represented the PSD of measured wall-pressure fluctuations at subsonic and supersonic speeds. Lowson's predicted auto-spectra has the form of Eq. (6),

$$\Phi(f) = \frac{{q_\infty}^2\left(\frac{\overline{P^2}}{{q_\infty}^2}\right)}{\omega_o\left(1 + \left(\frac{2\pi f}{\omega_o}\right)^2\right)^{\frac{3}{2}}} \quad (6)$$

where;

$$\omega_o = \frac{8U_\infty}{\delta}, \quad \frac{\overline{P^2}}{{q_\infty}^2} = \frac{(0.006)^2}{(1+0.14M^2)^2},$$

$$\delta = 0.37xR_{e_x}{}^{-\frac{1}{5}}\left[1 + \left(\frac{R_{e_x}}{2.9\,x\,10^7}\right)^2\right]^{\frac{1}{10}}$$

2.4 Robertson's Model [20]

Robertson extended the work of Lowson [19] using further subsonic and supersonic wind tunnel measurements. He proposed a slightly modified semi-empirical expression that improved upon the high-frequency roll-off, and increased spectrum amplitudes at low frequencies. The dimensional form of the predicted auto-spectra is given in Eq. (7),

$$\Phi(f) = \frac{{q_\infty}^2\left(\frac{\overline{P^2}}{{q_\infty}^2}\right)}{\omega_o\left(1 + \left(\frac{2\pi f}{\omega_o}\right)^{0.9}\right)^2} \quad (7)$$

where;

$$\omega_o = \frac{U_\infty}{2\delta^*}$$

The boundary layer thickness and displacement thickness were predicted using Eq. (7a) and Eq. (7b) respectively [26].

$$\delta = 0.37xR_{e_x}{}^{-\frac{1}{5}}\left[1 + \left(\frac{R_{e_x}}{6.9\,x\,10^7}\right)^2\right]^{\frac{1}{10}} \quad (7a)$$

$$\delta^* = \frac{\delta[1.3 + 0.43M^2]}{10.4 + 0.5M^2[\left[1 + 2x10^{-8}R_{e_x}\right]^{1/3}} \quad (7b)$$

2.5 Laganelli's Model [21]

Laganelli extended the work of Robertson [20] to account for viscous effects, compressibility and heat transfer of the medium. Using subsonic and supersonic wind tunnel measurements, Laganelli proposed a model in the form of Eq. (8),

$$\Phi(f) = \frac{q^2\delta^*(2.293\,x10^{-5}){F_c}^{-0.5733}}{U_\infty\left[1 + {F_c}^{2.867}\left(\frac{2\pi f\delta^*}{U_\infty}\right)^2\right]} \quad (8)$$

where; F_c is a transformation function from compressible to incompressible flow states, and can be calculated using Eq. (8a). For this study, on low Mach number flows, the ratio of h_w/h_{aw} was assumed to be unity.

$$F_c = \frac{1}{2} + \frac{h_w}{h_{aw}}\left(\frac{1}{2} + r\frac{\gamma - 1}{2}M^2\right) + 0.22r\frac{\gamma - 1}{2}M^2 \quad (8a)$$

2.6 Goody's Model [11]

More recent efforts by Goody were directed at modifying the Chase-Howe model to better agree with experimental measurements from a collection of sources. Goody noted that the Chase-Howe model under-predicted the spectral density levels at low frequencies and the slope of the roll-off at high frequencies. Goody postulated the model in Eq. (9) to correct the aforementioned shortcomings,

$$\Phi(f) = \frac{3(2\pi f\tau_w)^2\left(\frac{\delta}{U_\infty}\right)^3}{\left(\left(\frac{2\pi f\delta}{U_\infty}\right)^{\frac{3}{4}} + 0.5\right)^{3.7} + \left(1.1R_\tau{}^{-0.57}\left(\frac{2\pi f\delta}{U_\infty}\right)\right)^7} \quad (9)$$

where;

$$R_\tau = \left(\frac{U_\tau\delta}{\nu}\right)\sqrt{\frac{C_f}{2}},\ \tau_w = q_\infty C_f$$

2.7 Smol'yakov's Model [12]

Using several sets of experimental data from the literature, Smol'yakov developed a three-part model to represent the behaviour of the low-frequency, overlap, and high-frequency ranges. The first term describes the fundamental behaviour of the spectrum in each range, and the second term ($\{\ldots\}$), in Eq. (10a) and Eq. (10b), describes the transition between ranges. The low-frequency, overlap, and high-frequency spectral amplitudes can be predicted using Eq. (10a), Eq. (10b) and Eq. (10c), respectively.

$$\Phi(f) = \frac{1}{U_\tau^2} 1.49\text{x}10^{-5} \tau_w^2 \nu {R_\theta}^{2.74} \bar{f}^2 \left(1 - 0.117 {R_\theta}^{0.44} \bar{f}^{\frac{1}{2}}\right)$$

$$for\ \bar{f} < \bar{f}_o \tag{10a}$$

$$\Phi(f) = \frac{2.75\tau_w^2 \nu}{U_\tau^2 \bar{f}^{1.11}} \left\{1 - 0.82\exp\left[-0.51\left(\frac{\bar{f}}{\bar{f}_o} - 1\right)\right]\right\}$$

$$for\ \bar{f}_o < \bar{f} < 0.2 \tag{10b}$$

$$\Phi(f) = \frac{\tau_w^2 \nu\left(38.9\exp\left(-8.35\bar{f}\right) + 18.6\exp\left(-3.58\bar{f}\right) + 0.31\exp\left(-2.14\bar{f}\right)\right)}{U_\tau^2} \left\{1 - 0.82\exp\left[-0.51\left(\frac{\bar{f}}{\bar{f}_o} - 1\right)\right]\right\}$$

$$for\ \bar{f} > 0.2 \tag{10c}$$

where:

$$\bar{f} = \frac{2\pi f \nu}{U_\tau^2},\ \bar{f}_o = 49.35 {R_\theta}^{-0.88},\ R_\theta = \frac{U_\infty \theta}{\nu}$$

The momentum thickness was estimated using Eq. (11) from [26] with δ estimated using Eq. (7a).

$$\theta = \frac{\delta}{10.4 + 0.5M^2[1 + 2\text{x}10^{-8} R_{ex}]^{1/3}} \tag{11}$$

3 Experimental Setup

3.1 Test Bed and Instrumentation

The subsonic wind tunnel at Carleton University is a continuous flow, fan-driven system, operated using a digital control unit. The wind tunnel has a maximum flow speed of approximately 50 m/s (M ≅ 0.15) and the control unit is programmed for 0.9 m/s speed increments. Before entering the contraction, the airflow is filtered using a turbulence grid to reduce the freestream turbulence to less than 2.5%, as found in previous studies in the facility [27]. The flow is accelerated through the contraction into a custom two-piece, noise-reduction chamber with a constant cross-section of 0.80 m x 0.48 m. and a length of 1.83 m (Fig. 2).

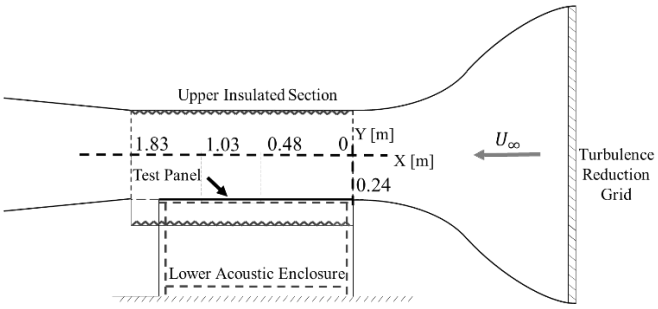

Figure 2: Schematic of wind tunnel test section

The upper section was lined with an acoustic foam in an attempt to reduce the intensity of the acoustic signatures from the wind tunnel motor and its controller, within the test section. The acrylic test panel was simply supported within floor of the test section, formed by the upper surface of an acoustically insulated box enclosing the microphones from the ambient environment.

The acrylic test panel was made 0.019 m thick to closely approximate an environment where the airborne noise can be examined in isolation from structure-borne noise; a key assumption associated with existing wall-pressure spectrum models. The panel was machined with a rectangular array of 25 threaded slots (Fig. 3) to accommodate microphones in various streamwise and spanwise configurations. Microphones are flush-mounted with the surface of the test panel using specialized, two-piece capsules, which house the microphones. Custom threaded plugs were designed to occupy the vacant holes in the panel.

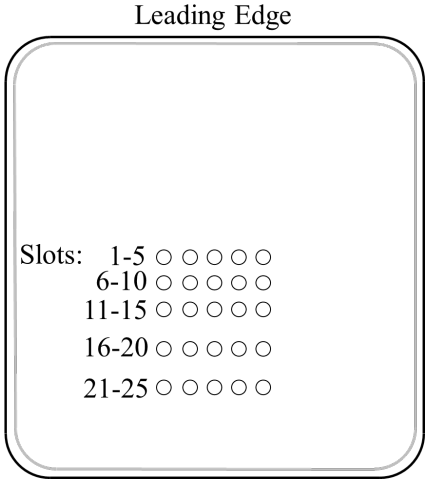

Figure 3: Schematic representation of acrylic test panel

The array permits wall-pressure measurements to be made over a span of 127 mm and 102 mm in the streamwise and spanwise directions, respectively. The first row of microphone slots were located 254 mm from the leading edge of the panel. A list of basic panel geometries is provided in Table 1.

Table 1: Panel geometry

Description	Value, m
Plate length	0.546
Plate width	0.448
Plate thickness	0.019
Spanwise array separation, typ.	0.025
Streamwise array separation (rows 1-3)	0.025
Streamwise array separation (rows 3-5)	0.038

Wall-pressure fluctuations were measured at position 23 on the panel, 0.86 m from the beginning of the test section, for Mach numbers of 0.06, 0.09 and 0.12. The reference microphone, used for signal processing was positioned in slot 21 on the panel. The formulas presented in Sec. 2 were used to predict the boundary layer properties over the test panel, which are summarized in Table 2. Note that the boundary layer was assumed to start from the inlet of the test section.

Table 2: Predicted boundary layer characteristics

Property	U_∞=20 m/s (M = 0.06)	U_∞=30 m/s (M = 0.09)	U_∞=40 m/s (M = 0.12)
$\delta_{Eq.(2a)}$ [mm]	20.1	18.5	17.5
$\delta_{Eq.(6)}$ [mm]	20.1	18.5	17.5
$\delta_{Eq.(7a)}$ [mm]	20.1	18.5	17.5
$\delta_{Eq.(4)}{}^*$ [mm]	3.1	2.7	2.5
$\delta_{Eq.(7a)}{}^*$ [mm]	2.5	2.3	2.2
θ [mm]	1.9	1.8	1.7
U_τ [m/s]	0.85	1.23	1.59

The microphone array consisted of two, ¼ in.-diameter, Brüel and Kjaer 4944A type microphones. The microphones have a flat frequency response, between 50 Hz and 10 kHz, with an upper dynamic frequency limit of 70 kHz and sensitivities of 0.90 mV/Pa and 0.83 mV/Pa (reference microphone). A single tone calibration, completed for each microphone, gave very similar sensitivities to the values provided by the manufacturer. Therefore, each pressure signal was corrected using the manufacturer's calibration specification. The environmental noise was filtered from the pressure signal (Sec. 3.3) using two microphones, placed at the same streamwise location on the panel, spaced 50.8 mm apart. The microphones were outfitted with standard grid caps and custom caps with a 0.5 mm diameter pinhole, shown schematically in Fig. 4.

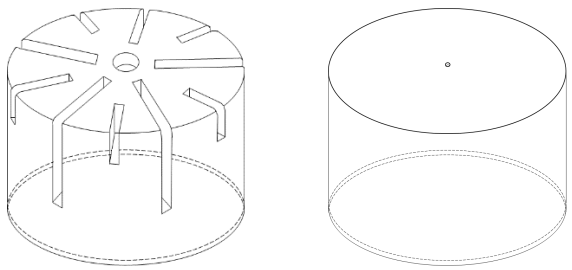

Figure 4: Schematic of microphone caps: a) standard grid cap and b) custom pinhole cap

This pinhole diameter has been found to be sufficient for accurately resolving the frequency spectrum up to 20 kHz [28]. The pinhole, having a diameter of 0.5 mm and a depth of 0.25 mm, enclosed a cavity above the microphone diaphragm having a depth of 1.4 mm and a width of 5.95 mm. The pinhole cap has an estimated Helmholtz resonance frequency of 15.7 kHz. The resonant frequencies for the grid cap are too complex to analytically predict, but resonance effects appear to set in above 4 kHz for M = 0.12 (see Fig. 6b), and as low as 2 kHz for M = 0.06. Therefore, measurements made with microphones outfitted with grid caps, were truncated to frequencies below the onset of resonance.

3.2 Acoustic Environment of the Wind Tunnel Test Section

Initial measurements with the microphones suggested that the acoustic signature of wind tunnel environment, from sources such as vibrations, turbulence filter screens, and the wind tunnel fan, had an impact on the measured spectra in the low frequency range (f < 250 Hz). Similar effects have been noted by others [29-31] and are common for in-flight measurements, which can be contaminated by low-frequency harmonics from the engines [32]. Other sources of noise, which contaminated the measurements, came from the fan-cooled wind tunnel controller unit. The cooling unit operates at a constant speed, and thus has a constant signature, which was removed from the measurements using pressure signals recorded with the microphones flush-mounted with the surface of the panel under quiescent flow conditions. To remove propagated wind tunnel environmental noise, a filtering technique was employed, using correlations between two microphones located at the same streamwise position, as described in Sec. 3.3.

3.3 Signal Processing

Wall-pressure fluctuations were recorded at 200 kHz for 25 seconds to produce a sufficiently large data set for temporal averaging (N = 5 x 10^6). The pressure signals were divided into 50 ensembles and averaged using non-overlapping Hamming windows [33]. Therefore, the averaged spectra were computed using 50 ensembles, each having a block length of 100,000.

To remove the propagated noise from the wind tunnel environment, a technique taken from [34] was employed. The measured pressure signal at any frequency, f, has the assumed composition of two separable components: propagated wind tunnel acoustic noise (subscript a), and turbulence-induced noise (subscript t) (Eq. (12)).

$$p_f = p_{af} + p_{tf} \tag{12}$$

For two microphones, placed at the same streamwise location, but separated by at least one length scale of the TBL, it is assumed that convected power of the propagated acoustic field is stronger than that due to turbulence in the spanwise direction. Then, turbulence-induced noise can be resolved through temporal subtraction of the pressure signal

obtained with the reference microphone (subscript 2), from that obtained at the location of interest (subscript 1), and taking the mean-square value of the result (Eq. (13)),

$$\overline{p_{1tf}^2} = \frac{1}{2}\overline{\left(p_{1f} - p_{2f}\right)^2} \quad (13)$$

since;

$\overline{p_{1tf}p_{2tf}} = 0$ (uncorrelated turbulent signals)
$\overline{p_{1tf}^2} = \overline{p_{2tf}^2}$ (two-dimensional and homogeneous flow)
$\overline{p_{1af}p_{2tf}} = \overline{p_{2af}p_{1tf}} = \overline{p_{1af}p_{1tf}} = \overline{p_{2af}p_{2tf}} = 0$
(uncorrelated wind tunnel acoustic, and turbulent signals)

This correction was applied to the recorded wall-pressure signals, measured at position 23 on the panel, using the pressure signal measured at position 21 as the reference for filtering. A sample of the time signals recorded from position 21 and position 23 are shown in Fig. 5.

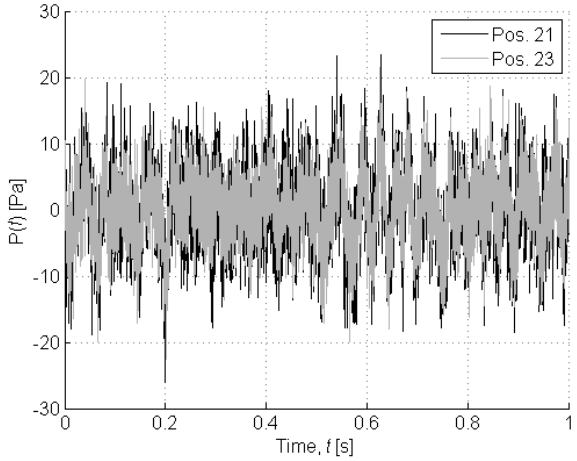

Figure 5: Sample of time signals recorded at position 21 and position 23 for M = 0.12

3.4 Microphone Signal Corrections

A microphone of finite size is limited in its ability to measure high-frequency pressure fluctuations, as its response is proportional to a spatial average of pressure over its face, causing the microphone to act as a low-pass filter [22,35-37]. Therefore, a correction must be applied to the measured high-frequency response. Corcos [22] theoretically formulated a model for characterizing, and correcting the response of a finite-sized transducer, for measuring pressure fluctuations in a TBL. The correction factor is calculated based on the cross-spectral response of the flow, the microphone response kernel, and the Strouhal number [22]. Corcos provides a tabulated list of correction factors, in ratio form of measured $(\Phi(\omega)_m)$ to actual $(\Phi(\omega))$ spectral behaviour, as a function of a similarity parameter, $\omega r/U_c$, assuming a uniform sensitivity across the sensing face of the transducer. The tabulated corrections were used to interpolate appropriate values for the complete frequency range. An example of the correction, for measurements with the pinhole and grid caps, are shown in Fig. 6a and Fig. 6b, respectively.

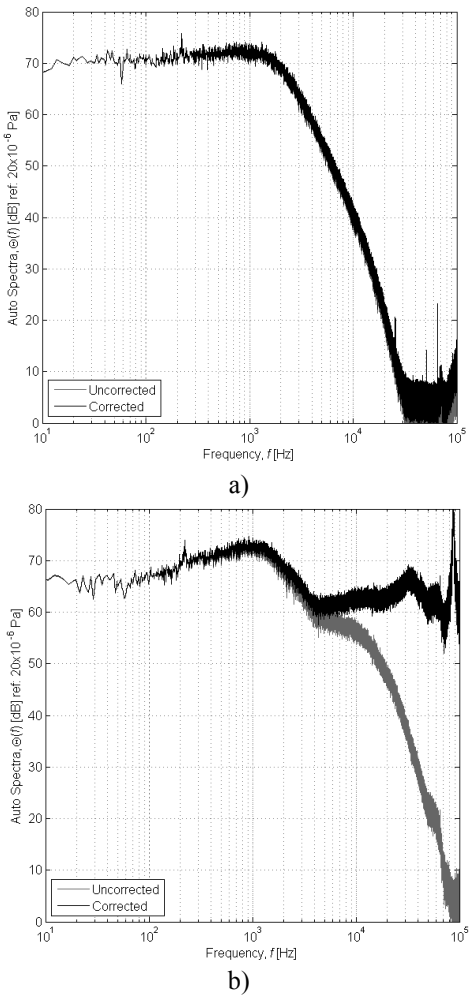

Figure 6: Corrected and uncorrected PSD measured using microphones outfitted with a) pinhole caps and b) standard grid caps

Although it is the most widely used correction for wall-pressure transducers, some have questioned the validity of the correction for high frequencies ($\omega r/U_c \geq 4$), and have related the applicability of the correction to various non-dimensional parameters [35-37]. For example, Schewe [35] proposed the use of a non-dimensional diameter, $\delta^+ = \delta U_\tau/\nu$, and claimed that the correction factor becomes inaccurate for $\delta^+ \geq 160$. The non-dimensional diameters for the grid cap and pinhole cap were calculated to be 641 and 51, respectively. Schewe's [35] criterion suggests that the Corcos correction cannot accurately predict the attenuation in the grid cap microphone measurements; therefore, the correction was only applied to pinhole microphone measurements for $\omega r/U_c \leq 4$.

4 Results and Discussion

4.1 Single-Point Frequency Spectra of Wall-Pressure Fluctuations

The auto-spectra for M = 0.06, 0.09 and 0.12, as measured with the microphones outfitted with grid caps and pinhole caps, are presented in Fig. 7 and Fig. 8, respectively.

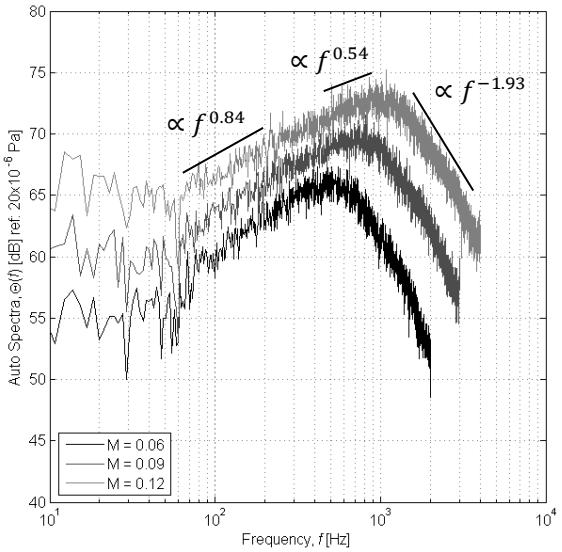

Figure 7: Progression of frequency spectra of wall-pressure fluctuations for Mach 0.06, 0.09 and 0.12 as measured with the grid cap microphone

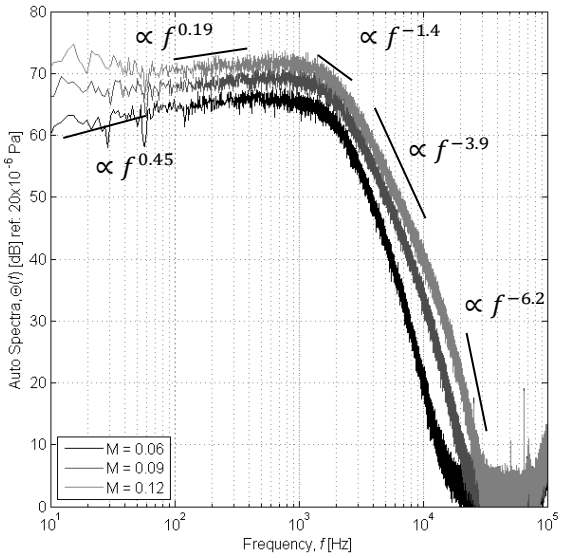

Figure 8: Progression of frequency spectra of wall-pressure fluctuations for Mach 0.06, 0.09 and 0.12 as measured with the pinhole microphone

As expected, the mean spectral density increases with increasing Mach number in all cases and both microphone configurations capture a spectral peak around 0.8-1 kHz. Regarding the spectrum shape, a well-behaved spectrum should exhibit the following characteristics: an increase in spectral energy, over the low-frequency range (f < 65 Hz) with a slope proportional to f^2 [38,39], followed by a continued increase up to 650 Hz in the mid-frequency range ($\propto f^{0.2}$ [40] or $\propto f^{0.3}$ [41]). The spectrum is then expected to decrease with a dependence of f^{-1} [1,8,38,39] over the overlap frequency range (1.3 kHz < f < 55 kHz); however, more recent experimental investigations suggest that the dependence can vary between $f^{-0.7}$ [11] and $f^{-1.11}$ [12]. The variations have been attributed by Smol'yakov [12] to an incompletely frozen pressure field and the spectral dependence on Reynolds number. The transition from the overlap range to high-frequency range (f > 55 kHz) has been found to occur with a slope around $f^{-\frac{7}{3}}$ [35], with the spectral roll-off slope typically reaching a dependence of f^{-5} [1,11,41].

In a wind tunnel environment it is very rare that the low-frequency spectra is accurately captured, due to propagated noise from the fan and structural vibration. Using the filtering method presented in Sec. 3.3, a spectral energy density was captured for frequencies as low as 1 Hz, however, neither spectra exhibited the expected slope proportional to f^2 in this range. The increasing spectral energy below 10 Hz could be a result of pressure fluctuations from irrotational motion of the flow above the boundary layer [8].

Over the mid-frequency range, the pinhole measurements were found to be in excellent agreement with expected trends, as the spectral energy slope was found to be proportional to $f^{0.19}$. The grid cap measurements show a greater spectral energy slope proportional to $f^{0.54}$, but one that remains on the order of magnitude of the expected trend.

Truncated measurements with the grid cap configuration show a spectral slope proportional to $f^{-1.93}$ beyond 1 kHz. This exceeds the commonly reported slope of f^{-1} over the overlap range, but was found to be in reasonable agreement with the findings of Schewe [35] for the transition between overlap- and high-frequency ranges. The spectra measured using the pinhole configuration are in reasonable agreement with the literature over the mid- and overlap-frequency ranges. The decay rate transitions through the brief overlap range, from $f^{-1.4}$ to $f^{-3.9}$ (2 kHz < f < 10 kHz), and eventually to $f^{-6.2}$ above 20 kHz. The measured decay rate in the high-frequency range was limited due to resonance effects above 20 kHz.

Both wall-pressure spectra exhibit marginal overlap regions. The behaviour of the spectra in this range is dependent on turbulent motion in the logarithmic region of the boundary layer between the inner, viscous layer and the outer wake layer. The Reynolds number is the most dominant variable for the width of the logarithmic region and the tendencies of the spectra have been studied using Re_θ, the Reynolds number based on momentum thickness, by several researchers [8,9,12,38]. Panton and Linebarger [38] postulated, and confirmed analytically, that there exists a critical value of Re_θ, below which, the effects of the logarithmic layer become negligible, causing the overlap range in the spectrum to disappear altogether. Farabee and Casarella [8], and Gravante et. al. [9], experimentally confirmed that the frequency range, over which the spectra exhibits the expected f^{-1} trend, decreases with decreasing Reynolds number, eventually becoming non-existent. According to Smol'yakov [12], $Re_\theta \leq 3.5 \times 10^3$ represents the critical value for the existence of an overlap region in the spectra. This would suggest that, for the flow conditions considered ($2.2\times10^3 \leq Re_\theta \leq 3.8\times10^3$), the logarithmic layer, and the TBL as a whole, may be marginally under developed. However, the

pinhole microphone configuration (Fig. 8) was capable of measuring a small overlap region, the shape of which, is in agreement with the measurements by Gravante et al. [9] for similar flow conditions.

4.2 Normalized Frequency Spectra

The self-similarity of the measured spectra was investigated by normalizing the data using a mixed combination of inner and outer boundary layer parameters: τ_w, U_τ, and δ, in the form of $\Phi(f)U_\tau/\tau_w^2\delta$, as a function of $2\pi f\delta/U_\tau$. The combination of inner and outer boundary layer flow parameters, δ/U_τ, were chosen as they have been shown in the literature to be most appropriate for scaling the spectra from both inner and outer flow structures [8,16,38]. However, it has been reported that no combination of scaling variables can satisfactorily collapse the complete frequency spectrum. The normalized spectra are shown in Fig. 9 and Fig. 10 as measured with the grid cap and pinhole configurations, respectively.

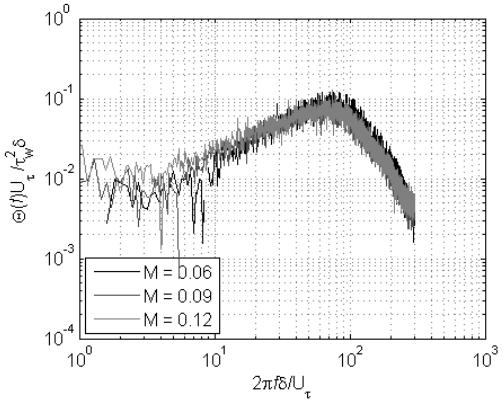

Figure 9: Normalized single-point wall-pressure spectrum as measured with the grid cap microphone

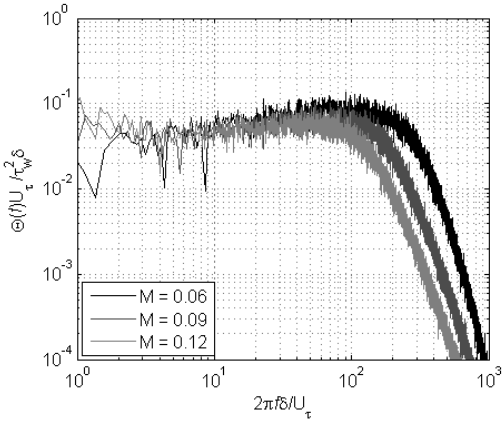

Figure 10: Normalized single-point wall-pressure spectrum as measured with the pinhole microphone

The non-dimensional spectra, measured with both configurations, collapse well over the mid-frequency range ($10 < 2\pi f\delta/U_\tau < 100$), however, less so for low frequencies. The outer-layer scaling set proposed by [10] ($\Phi(f)U_o/q_o^2\delta^*$ as a function of $2\pi f\delta^*/U_o$), were found to be equally acceptable over these ranges. The same scaling variables were also found to collapse the mid-frequency and overlap regions of the spectra in [8] and [16]. The normalized spectra measured with the pinhole microphone exhibit similar roll-off slopes however, the spectra show a Mach number dependence for $2\pi f\delta/U_\tau \geq 100$. The measured spectra with the grid cap microphone exhibit a much stronger self-similarity as they collapse well over the entire truncated frequency range. This is a result of scalable microphone attenuation disguised as flow-similarity. Signal attenuation is also responsible for the steeper spectral decay noted in Fig. 7. It is difficult to discern the frequency range over which the mixed-scaling variables are appropriate, since the grid cap measurements cannot offer confirmation over this range; similar to the spectra presented in [16]. That said, the inability to collapse the pinhole microphone spectra, over the overlap and high-frequency ranges, was not a shortcoming of the selected scaling variables since the data did not collapse using a set of inner variables ($\Phi(f)U_\tau^2/\tau_w^2\nu$ as a function of $2\pi f\nu/U_\tau^2$), which were found to be appropriate for these regions of the spectra by [1,8]. This would suggest that either the high-frequency regime may be sensitive to scaling based on measured versus predicted boundary layer properties, or the boundary layer was marginally under-developed, and therefore, does not exhibit self-similarity. Both should be investigated by experimentally characterizing the flow; however, the latter will have a greater influence on spectral self-similarity. With an under-developed boundary layer it becomes difficult to delineate between flow similarity and scaling parameter dependencies.

4.3 Comparison of Measured and Predicted Wall-Pressure Spectra

Fig. 11 and Fig. 12 show comparisons between the experimental wall-pressure spectra and a selection of existing semi-empirical models (Sec. 2), as measured using the grid cap and pinhole microphones, respectively.

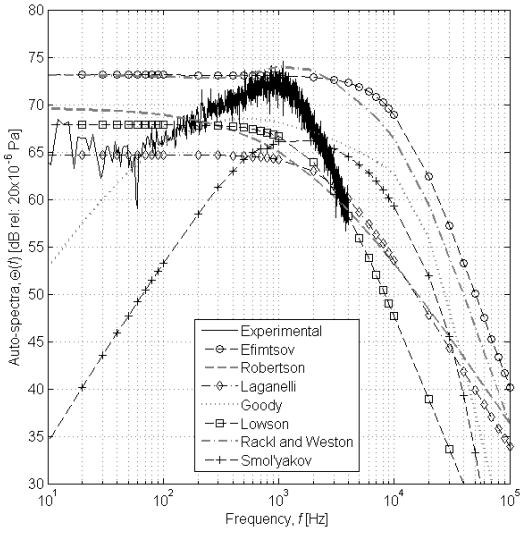

Figure 11: Wall-pressure spectrum for M = 0.12, as measured with the grid cap microphone, compared to existing semi-empirical models

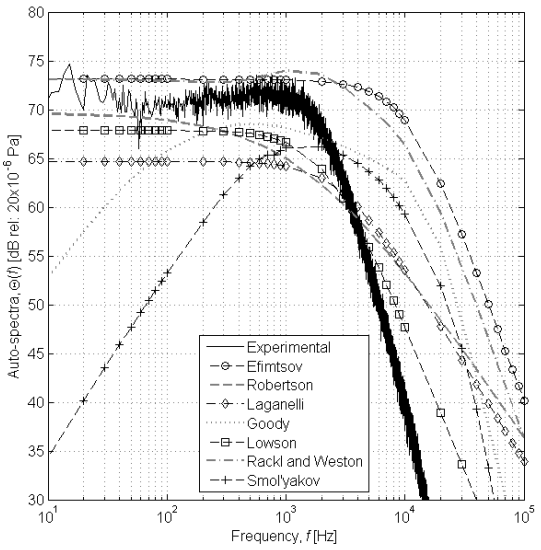

Figure 12: Wall-pressure spectrum for M = 0.12, as measured with the pinhole microphone, compared to existing semi-empirical models

From Fig. 12, one can see that the low- to mid-frequency spectrum is best predicted by the Efimtsov [17] and Rackl and Weston [18] empirical models. No model accurately predicts the steep roll-off beginning around 1 kHz; however, the overlap decay rate ($f^{-3.9}$) is best predicted by the Efimtsov model [17] ($f^{-3.1}$) and the more recent models of Goody [11] ($f^{-4.6}$) and Smol'yakov [12] ($f^{-4.7}$). The Goody model [11] is marginally more accurate at predicting the peak frequency near 0.8 kHz, compared to the Smol'yakov model [12]. The most apparent shortcoming of the more recent models is the under-prediction of spectral energy in the low- and mid-frequency regimes. The predicted spectrum from the Robertson model [20] and Laganelli model [21] do not compare well to either experimental spectra, in both shape and predicted levels. The Robertson model [20] does predict the spectrum levels at very low frequencies ($f < 100$ Hz); however, the experimental measurements in this range begin to deviate from the expected behaviour, which explains the agreement between the two in this frequency range. The Lowson model [19], a derivative of the Robertson model [20], under-predicts spectrum levels in the low- and mid-frequency ranges and the overlap decay rate ($f^{-3.0}$). The Rackl and Weston model [18] offers an improvement over the Efimtsov model [17] as, it too, predicts the shape of the spectra measured by the pinhole microphones in the low- and mid-frequency ranges, in addition to closely predicting the location of the spectral peak around 1 kHz. The modifications made by Rackl and Weston [18] force the predicted high-frequency slope ($f^{5.22}$) to better match the quoted f^{-5} in the literature, but tends to over-predict the measured decay rate in the overlap range, compared to that predicted by the Efimtsov model [17] ($f^{-3.1}$). Based on the pinhole measurements, which most closely exhibit the expected spectral features (Sec. 4.1), and cover a more complete frequency range, the models by Efimtsov [17] and Rackl and Weston [18], and Goody [11] and Smol'yakov [12], are most appropriate for predicting wall-pressure spectra over the low- to mid-frequency range, and overlap decay rate, respectively. However, since near-wall (high frequency), turbulent structures contribute most to the overall sound pressure levels, the more accurate prediction of Goody [11] and Smol'yakov [12] models in the overlap and high-frequency ranges may make them more preferable for low Mach number flows.

As the semi-empirical models are based on wall-pressure fluctuations beneath a fully developed TBL, they all account for an appreciable contribution from the overlap-region. Therefore, discrepancies between the measurements and model predictions are a result of the natural, under-developed logarithmic region of the boundary layer. As an example, a comparison of the normalized spectra, measured with the pinhole microphone, was made with the normalized spectra from Palumbo [41], at M = 0.76. Some spectrum features measured by Palumbo [41] are in good agreement with our measurements, such as the spectral peak around 1 kHz, the mid-frequency slope proportional to $f^{0.3}$, an overlap decay proportional to f^{-1}, and a high-frequency slope proportional to f^{5}. The major difference between the spectra is the existence of a sizeable overlap-region. Palumbo's [41] in-flight wall-pressure spectra is scaled using τ_w, U_τ, and δ, as before, and overlaid in Fig. 13 against our normalized spectra at M = 0.12, and the predictions from the models by Efimtsov [17], Rackl and Weston [18], Goody [11] and Smol'yakov [12].

From Fig. 13, one can see the effect of the presence of an overlap region on the agreement with the existing semi-empirical models. The greater spectrum energy in the overlap-region delays the roll-off and extends the spectral energy from the mid-frequency range by approximately 75% of a decade. The result is an excellent agreement with the models by Efimtsov [17] and Rackl and Weston [18] in the overlap frequency range.

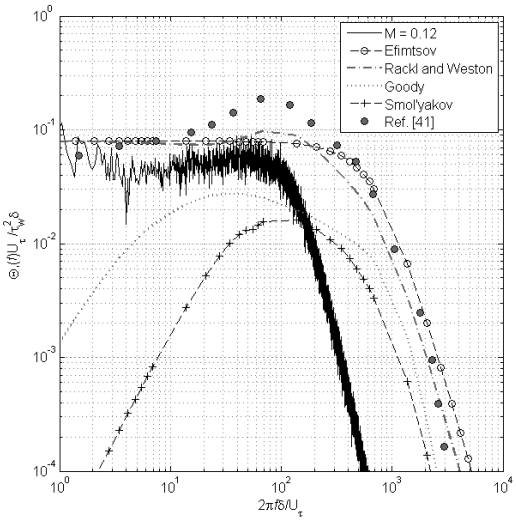

Figure 13: Normalized wall-pressure spectra compared with an experimental spectra from reference [41] and semi-empirical models

Literature suggests that with increasing Re_θ, the overlap range becomes more apparent and forces the roll-off to occur later [8,9]. Therefore, the implementation of a trip wire system will artificially increase Re_θ for the same mean flow speeds, thus delaying the high frequency roll-off, similar to Palumbo's data [41]. In turn, a closer match with the empirical models is expected. Based on this comparison with Palumbo [41], the agreement with the mid-frequency spectra and spectrum overlap decay rate measured with the pinhole cap configuration, it is conclude that the models by Efimtsov [17] and Rackl and Weston [18] are most appropriate for low Mach number flows.

5 Conclusions

Wall-pressure fluctuations were measured on a rigid acrylic panel beneath a turbulent boundary layer in Carleton University's subsonic wind tunnel facility, for Mach numbers ranging from M = 0.06 to 0.12. The upper frequency range of the grid cap configuration was limited by resonance occurring as low as 2 kHz at M = 0.06. Spectral growth and decay rates, measured with the pinhole microphones, were in better agreement with the expected behaviour reported in the literature over the mid- and overlap frequency ranges. Neither microphone configuration captured a significant overlap region. This was attributed to an under-developed logarithmic region of the boundary layer, which contributes significantly to spectra levels in the overlap range.

The spectra measured with the grid cap microphones were seen to scale well over the entire frequency range using inner and outer layer variables. The normalized spectra, measured with the pinhole microphone configuration, also scaled well using inner and outer variables over the mid-frequency range, but showed a Mach number dependence for over the overlap frequency range ($2\pi f\delta/U_\tau \geq 100$). This is also a result of the under-developed logarithmic region in the boundary layer, which does not exhibit self-similarity.

A selection of existing single-point frequency spectrum models, for turbulent boundary layer wall-pressure fluctuations, were reviewed and compared to spectra measured with both microphone cap configurations. The models by Efimtsov and Rackl and Weston best predict the spectra levels over the low- and mid-frequency ranges, and the overlap spectral energy decay rate is best predicted using the more recent models by Goody and Smol'yakov. The absence of a sizeable overlap region is responsible for the discrepancies between the measurements and predictions, beyond the spectral peak around 0.8 kHz.

Future work will include the use of a boundary layer trip system to fully develop the logarithmic-layer of the boundary layer. This will allow a more accurate simulation of TBL developed conditions in a laboratory. The flow should also be experimentally characterized to investigate the effects of measured versus predicted boundary variables for spectral scaling. A recessed microphone approach will be considered to eliminate resonance effects caused by the flush-mounted grid caps, and corroborate spectra scaling trends above 2 kHz.

Acknowledgements

The authors are grateful for the support from the Natural Sciences and Engineering Research Council of Canada, and collaboration with Bombardier Aerospace.

References

[1] M. Bull, "Wall-pressure fluctuations beneath turbulent boundary layers: some reflections on fourty years of research," *Journal of Sound and Vibration*, 190 :3, pp. 299-315, 1996.

[2] J. Wilby, "Aircraft interior noise," *Journal of Sound and Vibration*, 190 :3, pp. 545-564, 1996.

[3] J. Wilby and F. Gloyna, "Vibration measurements of an airplane fuselage structure: 1 - Turbulent boundary layer excitation," *Journal of Sound and Vibration*, 23 :4, pp. 443-466, 1972.

[4] R. Hayden, B. Murray and M. Theobald, "A Study of Interior Noise Levels, Noise Sources and Transmission Paths in Light Aircraft," NASA CR-172152, 1983.

[5] L. Maestrello, "Measurement of noise radiated by boundary layer excited panels," *Journal of Sound and Vibration*, 2: 2, pp. 100-115, 1965.

[6] M. Bull, "Properties of the fluctuating wall-pressure field of a turbulent boundary layer," *Advisory Group for Aeronautical Research and Development - Rpt. 455*, 1963.

[7] W. Blake, "Turbulent boundary-layer wall-pressure fluctuations on smooth and rough walls," *Journal of Fluid Mechanics*, 44 :4, pp. 637-660, 1970.

[8] T. Farabee and M. Casarella, "Spectral features of wall pressure fluctuations beneath turbulent boundary layers," *Physics of Fluids*, 3 :10, pp. 2410-2420, 1991.

[9] S. Gravante, A. Naguib, C. Wark and H. Nagib, "Characterization of the Pressure Fluctuations Under a Fully Developed Turbulent Boundary Layer," *AIAA Journal*, 36 :10, pp. 1808-1816, 1998.

[10] W. Keith, D. Hurdis and B. Abraham, "A comparison of turbulent boundary layer wall-pressure spectra," ASME, *Journal of Fluids Engineering*, 114 :3, pp. 338-347, 1992.

[11] M. Goody, "Empirical spectral model of surface pressure fluctuations," *AIAA Journal*, 42 :9, pp. 1788-1794, 2004.

[12] A. Smol'yakov, "Calculation of the Spectra of Pseudosound Wall-Pressure Fluctuations in Turbulent Boundary Layers," *Acoustical Physics*, 46 :3, pp. 342-347, 2000.

[13] J. da Rocha, A. Suleman and F. Lau, "Prediction of Flow-Induced Noise in Transport Vehicles: Development and Validation of a Coupled Structural-Acoustic Analytical Framework," *Canadian Acoustics*, 37 :4, pp. 13-29, 2009.

[14] J. da Rocha, A. Suleman and F. Lau, "Turbulent Boundary Layer Induced Noise and Vibration of a Multi-Panel Walled Acoustic Enclosure," *Canadian Acoustics*, 38 :4, pp. 9-22, 2010.

[15] Y. Hwang, W. Bonness and S. Hambric, "Comparison of semi-empirical models for turbulent boundary layer wall pressure spectra," *Journal of Sound and Vibration*, 319 :1-2, pp. 199-217, 2009.

[16] T. Miller, J. Gallman and M. Moeller, "Review of Turbulent Boundary-Layer Models for Acoustic Analysis," *Journal of Aircraft*, 49 :6, pp. 1739-1754, 2012.

[17] B. Efimtsov, "The Prediction of the Pressure Fluctuation Field Characteristics of the TBL", TsAGI, Contract No. BTRC-101F, Document No. BTRC101F-5/95, 1995.

[18] R. Rackl and A. Weston, "Modeling of Turbulent Boundary Layer Surface Pressure Fluctuation Auto and Cross Spectra -

Verification and Adjustments Based on TU-144LL Data," NASA/CR-2005-213938, Langley, Virginia, USA, 2005.
[19] M. Lowson, "Prediction of Boundary Layer Pressure Fluctuations," Air Force Flight Dynamics Laboratory - AFFDL-TR-67-167, Ohio, 1968.
[20] J. Robertson, "Prediction of in-flight fluctuating pressure environments including proturbence induced flow," Wyle Laboratories Research Staff Report, WR71-10, 1971.
[21] A. Laganelli and H. Wolfe, "Prediction of Fluctuating Pressure in Attached and Separated Turbulent Boundary-Layer Flow," *Journal of Aircraft*, 30:6, pp. 962-970, 1993.
[22] G. Corcos, "Resolution of Pressure in Turbulence," *The Journal of the Acoustical Society of America*, 35: 2, pp. 192-199, 1963.
[23] G. Corcos, "The structure of the turbulent pressure field in boundary-layer flows," *Journal of Fluid Mechanics*, 18 :3, pp. 353-378, 1964.
[24] R. Wahidi, W. Chakroun, A. Al-Fahed, "The behaviour of the skin-friction coefficient of a turbulent boundary layer flow over a flat plate with differently configured transverse square grooves", *Experimental Thermal and Fluid Sciences*, 30: 2, pp. 141-152, 2005.
[25] S. Rizzi, R. Rackl and E. Andrianov, "Flight Test Measurements From The Tu-144LL Structure/Cabin Noise Experiment," NASA/TM-2000-209858, 2000.
[26] D. Bies, "A review of flight and wind tunnel measurements of boundary layer pressure fluctuations and induced structural response," NASA CR-626, Langley, Virginia, USA, 1965.
[27] Roberts, S.K., Boundary layer Transition in Attached and Separated Flows at Low Reynolds Numbers, Ph.D thesis, Carleton University, 2005.
[28] W. Devenport, D. Grissom and W. Alexander, "Measurements of roughness noise," *Journal of Sound and Vibration*, 330 :17, pp. 4250-4273, 2011.
[29] W. Willmarth and C. Wooldridge, "Measurements of the fluctuating pressure at the wall beneath a thick turbulent boundary layer," *Journal of Fluid Mechanics*, 14 :2, pp. 187-210, 1962.
[30] M. Bull, "Wall-pressure fluctuations associated with subsonic turbulent boundary layer flow," *Journal of Fluid Mechanics*, 28 :4, pp. 719-754, 1967.
[31] J. Forest, The Wall-Pressure Spectrum of High Reynolds Number Rough-Wall Turbulent Boundary Layers, Master's Thesis, Virginia Tech Polytechnic Institute and State University, Blacksburg, VA, 2012.
[32] W. Brat, "Flight test measurement of exterior turbulent boundary layer pressure fluctuations on Boeing model 737 airplane," *Journal of Sound and Vibration*, 14 :4, pp. 439-457, 1971.
[33] N. S. Corporation, Power Spectra Estimation, AN-255, 1980.
[34] R. Simpson, M. Ghodbane and B. McGrath, "Surface pressure fluctuations in a separating turbulent boundary layer," *Journal of Fluid Mechanics*, 177, pp. 167-186, 1987.
[35] G. Schewe, "On the structure and resolution of wall-pressure fluctuations associated with turbulent boundary layer flow," *Journal of Fluid Mechanics*, 134, pp. 311-328, 1983.
[36] F. Geib, "Measurements on the Effect of Transducer Size on the Resolution of Boundary-Layer Pressure Fluctuations," *The Journal of the Acoustical Society of America*, 46 :1B, pp. 253-261, 1969.
[37] R. Lueptow, "Transducer resolution and the turbulent wall pressure spectrum," *The Journal of the Acoustical Society of America*, 97 :1, pp. 370-378, 1995.
[38] R. Panton and J. Linebarger, "Wall pressure spectra calculations for equilibrium boundary layers," *Journal of Fluid Mechanics*, 65 :2, pp. 261-287, 1974.
[39] P. Bradshaw, D. Ferriss and N. Atwell, "Calculation of boundary-layer development using the turbulent energy equation," *Journal of Fluid Mechanics*, 28 :3, pp. 593-616, 1967.
[40] D. Leclercq and X. Bohineust, "Investigation and modelling of the wall pressure field beneath a turbulent boundary layer at low and medium frequencies," *Journal of Sound and Vibration*, 257 :3, pp. 477-501, 2002.
[41] D. Palumbo, "Determining correlation and coherence lengths in turbulent boundary layer flight data," *Journal of Sound and Vibration*, 331: 16, pp. 3721-3737, 2012.